


Article

# Electrophysiological Effects of Extracellular Vesicles Secreted by Cardiosphere-Derived Cells: Unraveling the Antiarrhythmic Properties of Cell Therapies

Lidia Gómez-Cid <sup>1,2,3</sup>, Marina Moro-López <sup>1,2</sup>, Ana S. de la Nava <sup>1,3,4</sup>,  
Ismael Hernández-Romero <sup>5</sup> , Ana I. Fernández <sup>1,3</sup>, Susana Suárez-Sancho <sup>1,3</sup>,  
Felipe Atienza <sup>1,3,6</sup>, Lilian Grigorian-Shamagian <sup>1,3,\*</sup> and Francisco Fernández-Avilés <sup>1,3,6</sup>

- <sup>1</sup> Instituto de Investigación Sanitaria Gregorio Marañón, Hospital Gregorio Marañón, 28009 Madrid, Spain; ligomezc@ing.uc3m.es (L.G.-C.); marina.moro@alumnos.uc3m.es (M.M.-L.); ansan38a@doctor.upv.es (A.S.d.l.N.); anaisabel.fernandez@ciber cv.es (A.I.F.); ssuarez@fibhgm.org (S.S.-S.); felipe.atienza@salud.madrid.com (F.A.); francisco.fernandezaviles@salud.madrid.org (F.F.-A.)
  - <sup>2</sup> Departamento de Bioingeniería e Ingeniería Aeroespacial, Universidad Carlos III de Madrid, 28911 Leganés, Spain
  - <sup>3</sup> CIBERCV, ISCIII, 28029 Madrid, Spain
  - <sup>4</sup> ITACA Institute, Universitat Politècnica de València, 46022 Valencia, Spain
  - <sup>5</sup> Department of Signal Theory and Communications, Universidad Rey Juan Carlos, 28943 Fuenlabrada, Spain; ismael.hernandez@urjc.es
  - <sup>6</sup> Faculty of Medicine, Universidad Complutense de Madrid, 28040 Madrid, Spain
- \* Correspondence: lgrigorian@ciber cv.es

Received: 30 June 2020; Accepted: 28 July 2020; Published: 2 August 2020



**Abstract:** Although cell-based therapies show potential antiarrhythmic effects that could be mediated by their paracrine action, the mechanisms and the extent of these effects were not deeply explored. We investigated the antiarrhythmic mechanisms of extracellular vesicles secreted by cardiosphere-derived cells (CDC-EVs) on the electrophysiological properties and gene expression profile of HL1 cardiomyocytes. HL-1 cultures were primed with CDC-EVs or serum-free medium alone for 48 h, followed by optical mapping and gene expression analysis. In optical mapping recordings, CDC-EVs reduced the activation complexity of the cardiomyocytes by 40%, increased rotor meandering, and reduced rotor curvature, as well as induced an 80% increase in conduction velocity. HL-1 cells primed with CDC-EVs presented higher expression of *SCN5A*, *CACNA1C*, and *GJA1*, coding for proteins involved in  $I_{Na}$ ,  $I_{CaL}$ , and Cx43, respectively. Our results suggest that CDC-EVs reduce activation complexity by increasing conduction velocity and modifying rotor dynamics, which could be driven by an increase in expression of *SCN5A* and *CACNA1C* genes, respectively. Our results provide new insights into the antiarrhythmic mechanisms of cell therapies, which should be further validated using other models.

**Keywords:** cell therapy; extracellular vesicles; antiarrhythmic effects; optical mapping; conduction velocity

## 1. Introduction

Tachyarrhythmias are variations that increase the normal heart rate without a physiological justification [1], and they are classified into supraventricular and ventricular arrhythmias according to their origin [2]. They affect over 2.2% of the population [3], and they are one of the main causes of morbidity and mortality worldwide [4]. Clinically, they can manifest as heart failure, chest pain,

weakness, syncope, cardiomyopathy, and even cardiac arrest and death [5]. Despite their high prevalence and impact, current treatments are still suboptimal [4].

To improve treatment efficacy, an understanding of the physiological mechanisms behind the tachyarrhythmias becomes essential [6]. The two main pointed mechanisms are enhanced impulse formation and conduction disturbances. Contrary to impulse formation, conduction disturbances produce so-called reentrant arrhythmias, in which the arrhythmia is commonly both initiated and sustained [1]. Rotors (spiral wave reentries that rotate around anatomical points) can occur around anatomical or functional obstacles, such as fibrotic regions, but their initiation and maintenance success is tightly related to low conduction velocity [1,7] and short action potential duration [8].

Despite some studies reducing arrhythmogenicity by improving conduction velocity [9,10], antiarrhythmic drugs used in the clinic do not currently act through this mechanism [11,12]. Conduction velocity in the cardiac tissue is mainly determined by the presence of gap junctions and by the late sodium current ( $I_{Na}$ ). Gap junctions play an important role in action potential propagation between cardiomyocytes [10,13], as they allow the passage of ions between different cells [14].

Shortening of the action potential durations is associated with shorter refractory periods and larger rotor stability [15]. Low L-type calcium current ( $I_{CaL}$ , determined by the presence of voltage-dependent L-type calcium channels coded by the *CACNA* family), is related to shorter action potential durations [16] (p. 187) and decreased meandering [17], leading to more rotor stability. Decreased meandering and an increase in rotor curvature reduce the probability of collision with other rotors and reduce the area needed for the rotor to self-sustain, increasing the number of possible simultaneous rotors in a certain area. These rotor dynamics related to shorter action potentials and low conduction velocities allow for a larger number of reentries in the cardiac tissue, leading to a larger activation complexity [18] (p. 347). This increase in complexity, as a more arrhythmogenic profile, is related to longer arrhythmia sustainment and lower ablation success [19].

Most pharmacologic therapies act by modulating or blocking ion channels, but do not correct the underlying causes [20]. On the other hand, ablation therapy produces irreversible changes in the cardiac substrate that limit its long-term success and its use in complex activation cases [21]. The efficacy of ablation and pharmacological therapies for tachyarrhythmias could be eventually optimized by emerging biological therapies, capable of modifying the pathophysiological substrate [20]. Some studies showed the antiarrhythmic properties of mesenchymal stem cells (MSCs) [22–26] or cardiosphere-derived cells (CDCs) [27,28], while others demonstrated pro-arrhythmic effects [29,30]. While the topic is still controversial, most of this proarrhythmicity is associated with stem cell engraftment itself and the alteration of the overall tissue excitability, as these effects are not observed or seem to be opposite when their paracrine factors are used instead [25,29]. Extracellular vesicles (EVs) are the main paracrine mediators of stem cells [31,32], and their use as therapeutics may have advantages compared to their parenteral cells [33,34]. It was demonstrated that blocking production of EVs renders CDCs ineffective, whereas CDC-EVs reproduce the benefits of the parent CDCs [32,33], as well as cardiac progenitor cells with broad-ranging bioactivity in preclinical and clinical studies [35,36].

Therefore, a deeper understanding and exploration of the mechanisms behind the potential antiarrhythmic effects of EVs secreted by cardiac stem cells and whether these are comparable to antiarrhythmic drugs could contribute to the development of more effective antiarrhythmic therapeutics. The objective of this study was to investigate the antiarrhythmic effects of extracellular vesicles secreted by human CDCs (CDC-EVs) on the cardiomyocyte monolayer presenting spontaneous arrhythmogenic activity and to elucidate the underlying antiarrhythmic mechanisms.

## 2. Materials and Methods

### 2.1. CDCs and Derived Extracellular Vesicle Isolation

Extracellular vesicles (EVs) used as treatment were isolated from CDCs from two different human donors. Half of the CDC-EV plates were treated with EVs from one donor, and the other half were treated with CDC-EVs from the other donor. No significant differences in proliferation, electrophysiological properties (i.e., activation complexity, dominant frequency, rotor dynamics, and conduction velocity), and gene expression profile were observed between the two donors. The process of CDC obtainment, illustrated in Figure 1, was described in detail by Smith et al. [37]. In brief, cardiac biopsies from patients undergoing cardiac surgery were processed through mechanical and enzymatic digestion to obtain explants of 1–2 mm. The explants were cultured over fibronectin-coated plates in Iscove's Modified Dulbecco's Medium (IMDM) supplemented 20% with Fetal Bovine Serum (FBS). Explant-derived cells (EDCs) started leaving the explant and colonizing the plate after approximately 48 h of culture, and they reached full confluency after approximately 16 days. Then, cells were transferred at a density of 25,000 cells/cm<sup>2</sup> to ultra-low-attachment Nunclon Plates for 72 h to allow them to form three-dimensional (3D) spheroids (cardiospheres), which are known to potentiate stemness and regenerative potential [37]. The cardiospheres were passaged to produce the CDCs, and their identity was confirmed by flow cytometry (0.9% CD45+ cells, 10.6% CD90+ cells, 6.6% CD117+ cells, 99.8% CD105+ cells, and 7.4% CD31+ cells). When CDCs-P3 reached 80% confluence, the medium was changed to FBS-free IMDM and left unchanged for 15 days to allow CDCs to secrete and concentrate EVs in the medium. Conditioned medium was filtrated using a 0.45- $\mu$ m filter and ultraconcentrated using Centricon-Plus 70 Centrifugal Filter with 3-kDa cut-off frequency (Merck KGaA, Darmstadt, Germany). EVs were then analyzed by nanoparticle tracking analysis (NTA, performed with NanoSight NS300 from Malvern Panalytical Ltd., Malvern, United Kingdom), and their protein content was determined with Bradford assay after EV lysis and protease inactivation. EVs were precipitated after incubation with 4% *w/v* polyethylene glycol (PEG) overnight at 4 °C and centrifugation at 4 °C at 1500 $\times$  *g* for 30 min. For experiments, the precipitated EVs were resuspended in Claycomb medium without FBS at 100  $\mu$ g/mL.

### 2.2. Experimental Protocol

The overall experimental protocol is summarized in Figure 2a. After CDC-EV isolation and quantification, HL-1 cells were plated in 35-mm-diameter petri dishes at a density of 26,000 cells/cm<sup>2</sup> and maintained according to the protocol established by Claycomb et al. [38]. Spontaneous beating activity was observed during cell expansion. When cultures reached a confluency of 80% (two days after plating), the culture medium was changed to serum-free medium, resulting in a control group and an EV group (with EVs resuspended in the serum-free medium). Fully confluent cultures were analyzed with the optical mapping (OM) technique, obtaining recordings of 20 s (*N* = 12 in control and *N* = 12 in CDC-EV group). After OM, cells were lysed and kept for further gene expression analysis in order to contrast the electrophysiological results with cardiac remodeling at the molecular level.

### 2.3. Optical Mapping Recordings

Cell cultures were stained with rhod-2 AM (Ca<sup>2+</sup>-sensitive probe) fluorescent dye prior to the calcium transient (CaT) imaging so that the propagation patterns could be recorded. HL-1 cells were incubated in serum-free media with rhod-2 (AAT Bioquest) at 3.3  $\mu$ M (from 1 mM aliquots in dimethyl sulfoxide, DMSO) and Probenecid (AAT Bioquest) at 1.75 mM (from 265 mM aliquots in Tyrode solution) for 30 min at 37 °C and 5% CO<sub>2</sub>. After dye loading, the serum-free medium was changed to fresh Tyrode solution (containing, in mM, NaCl 130, NaHCO<sub>3</sub> 24, NaH<sub>2</sub>PO<sub>4</sub>·H<sub>2</sub>O 1.2, MgCl<sub>2</sub> 1, KCl 4, glucose 5.6, and CaCl<sub>2</sub> 2.3) at physiological temperature.

To excite rhod-2, cultures were illuminated with a green light-emitting diode light source with a plano-convex lens and a green excitation filter. Fluorescence was recorded with an electron-multiplying charge-coupled device with a custom emission filter and a high-speed camera lens as described in

Reference [39]. Basal recordings of fluorescence were acquired at 50 frames/s and a field of view of  $\sim 2 \times 2 \text{ cm}^2$ . To facilitate linear propagation for velocity measurement, cell cultures were delimited in rectangular areas and stimulated with pulses of 40 V amplitude, 4 ms width, and 1 Hz pacing period.

#### 2.4. Calcium Image Processing

Electrophysiological properties of cell cultures were analyzed by processing CaT recordings as illustrated in Figure 2b with custom software written in MATLAB, quantifying dominant frequency (DF), complexity, curvature, rotor meandering, and CV as described by Climent et al. [39,40].

##### 2.4.1. Spectral Analysis

Power spectra were obtained using a Welch periodogram (2-s Hamming window overlap). DF for each pixel was defined as the frequency with the largest peak in the power spectrum, and DF for each culture was calculated as its maximum DF value.

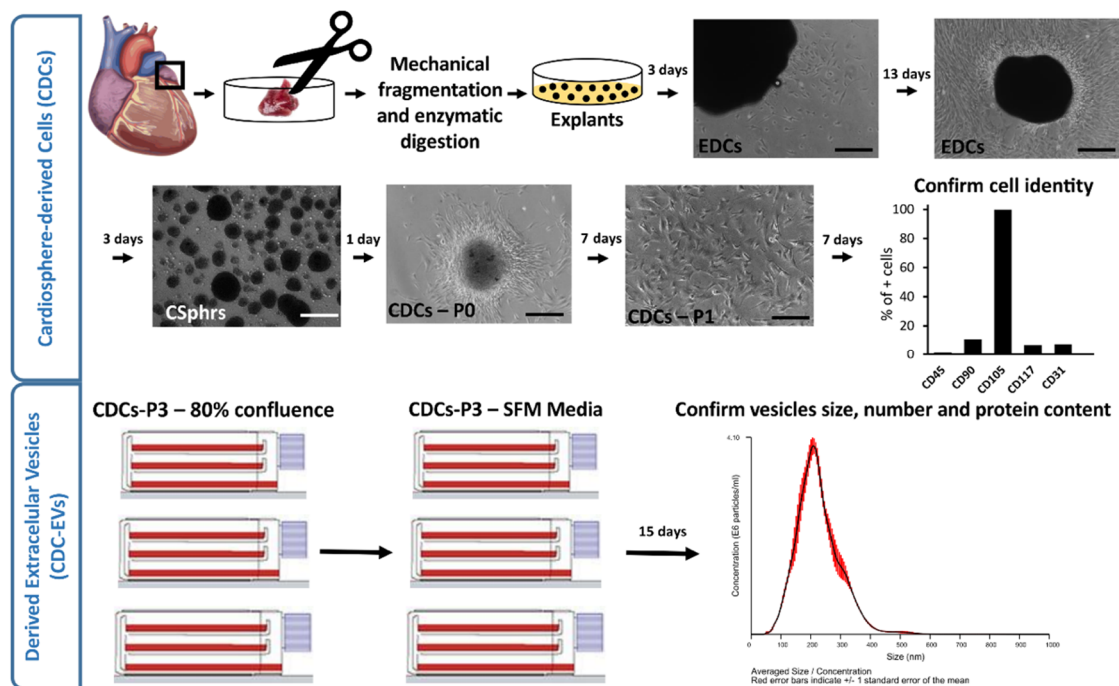


**Figure 1.** Methodology employed for cardiosphere-derived cell extracellular vesicle (CDC-EV) isolation. Scale bars correspond to 200  $\mu\text{m}$ . Cardiac biopsies from patients were immediately processed through mechanical and enzymatic digestion to obtain explants of 1–2 mm. Explant-derived cells (EDCs) started leaving the explant and colonizing the plate after approximately 48 h of culture and reached full confluency after approximately 16 days. Then, the cells were transferred to ultra-low-attachment plates for 72 h to allow them to form three-dimensional (3D) spheroids (cardiospheres). Cardiospheres were passaged to produce the so-called cardiosphere-derived cells (CDCs-P0). Cell identity was confirmed by flow cytometry in CDCs-P1 cells, with 0.9% CD45+ cells, 10.6% CD90+ cells, 6.6% CD117+ cells, 99.8% CD105+ cells, and 7.4% CD31+ cells. CDCs were further passaged until CDCs-P3 reached 80% confluence. At that point, the medium was changed to FBS-free IMDM and left unchanged for 15 days to allow CDCs to secrete and concentrate EVs in the medium. Conditioned medium was filtrated and ultraconcentrated, and EVs were precipitated and further resuspended. Quantification was performed through nanoparticle tracking analysis (NTA). The average particle size was 200  $\mu\text{m}$  and the maximum particle size was 450  $\mu\text{m}$ .

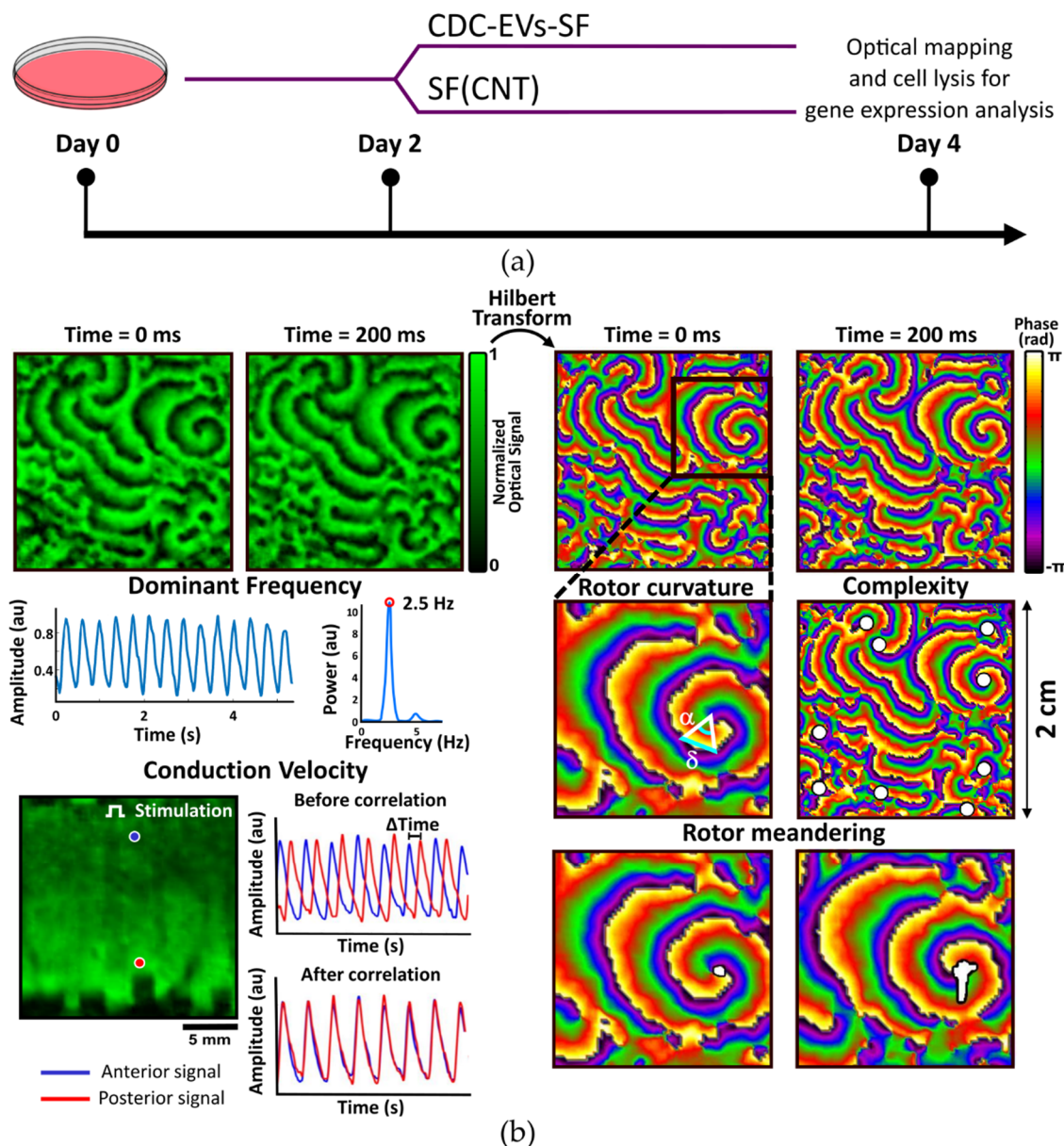


**Figure 2.** Experimental protocol and methodology employed for calcium transient (CaT) recording analysis: (a) experimental set-up consisting of cell seeding at day 0, Claycomb medium without FBS (serum-free (SF)) and with addition of EVs in CDC-EV group at day 2, and optical mapping and cell lysis for later RNA extraction at day 4; (b) example of optical mapping recording analysis. Two snapshots of optical mapping recordings are shown at 0 and 200 ms (upper left), as well as their phase maps, obtained by applying Hilbert transform (upper right). Example of the optical mapping signal for a specific pixel and its corresponding power spectrum, with the peak marking the dominant frequency, are shown (middle left). For conduction velocity (CV) (lower left), the culture is divided into delimited areas, and two pixels are selected (with their corresponding optical mapping signals). Correlation of these signals gives the time elapsed ( $\Delta t$ ) between the activation of the two points. CV is calculated as the ratio between the physical distance between the two points and the time elapsed. Rotor curvature, complexity, and meandering calculated from phase maps are represented. Rotor curvature was determined from the derivative of the relative angle ( $\alpha$ ) over the relative distance ( $\delta$ ) in lines from the rotor tip to  $2\pi$  (middle right). For complexity, phase singularities (PSs) were identified and quantified in a certain area (middle right). In rotor meandering, from the phase map, the path followed by the tip was traced and quantified (lower right).

#### 2.4.2. Phase Singularities and Rotor Dynamics

Phase maps were obtained by applying Hilbert transform to CaT signals, defining phase singularities (PSs) as points surrounded by phases from 0 to  $2\pi$  monotonically changing. Complexity was defined as the mean number of simultaneous functional reentries in a certain area (PS/cm<sup>2</sup>).

For curvature measuring, lines connecting phase transitions from 0 to  $2\pi$  were traced from the rotor tip to the periphery. The curvature of the rotor was the mean of the curvatures at each point, which were calculated as the derivative of the relative angle ( $\alpha$ ) over the relative distance ( $\delta$ ).

Rotor meandering was defined as the distance covered by the rotor tip over PS duration (cm/s). From the phase map, the path followed by the tip was traced and quantified. Meandering in each cell culture was calculated as the mean value of the meandering of all the PS.

#### 2.4.3. Conduction Velocity

CV was defined as the distance traveled by the linear propagation front (cm/s) in areas that only allowed unidirectional propagation. CaT signals from pixels at a known spatial distance were correlated to obtain time elapsed between their activations ( $\Delta t$ ). CV was calculated as the distance between the pixels divided by the elapsed time. For each culture, mean CV was computed with a minimum of eight delimited areas.

#### 2.5. Gene Expression Analysis

RNA of cell cultures was isolated using QIAzol Lysis Reagent (QIAGEN, Venlo, The Netherlands) and relative gene expression quantification was performed with a two-step RT-PCR. One microgram of total RNA was reverse-transcribed into complementary DNA (cDNA) using the iScript<sup>TM</sup> cDNA Synthesis Kit and random hexamer primers in 20- $\mu$ L reactions, following the manufacturer's instructions. cDNA obtained was diluted 1:20, and gene expression quantification was performed in a CFX Real-Time PCR Detection System (Bio-Rad Laboratories) using a 96-well plate where each sample was analyzed in triplicate. PCR amplifications were done with 2  $\mu$ L of diluted cDNA using SYBR Green chemistry and specific primer pairs (Supplementary Materials, Table S1) in a final volume of 20  $\mu$ L. RT-qPCR efficiency for each assay was controlled using relative standard curves generated from a pool of cDNA. Ct data was collected and analyzed applying the  $2^{-\Delta\Delta C_t}$  method for relative quantification using the sample with the highest expression as calibrator. Gene expression normalization factor was calculated for each sample based on the geometric mean of *GUSB* and *36B4* reference genes in geNorm [41].

The genes under study—*SCN5A*, *CACNA1C*, and *GJA1*—encode for proteins related to cardiac impulse propagation and involved in different ion currents and channels: voltage-activated sodium current ( $I_{Na}$ ), L-type calcium current ( $I_{CaL}$ ), and connexin 43 (Cx43), respectively.

#### 2.6. Statistical Analysis

Results are presented as mean  $\pm$  standard deviation in the text and  $\pm$  standard error of the mean in figures. Continuous variables were compared using Student's *t*-tests. Pearson tests were performed to study the correlation among the different electrophysiological parameters and between gene expression.

### 3. Results

CDC-EVs seem to drive HL-1 cells to a less arrhythmogenic profile. Figure 3 shows the comparison of the complexity, the dominant frequency, rotor dynamics, and conduction velocity for control vs. treated with CDC-EV HL-1 cell monolayers to illustrate the differences in their electrophysiological properties. The corresponding graphs summarizing the results, as well as representative images of culture wells in both groups, are also shown. The plates were fully confluent during optical

mapping recordings (plates in both groups reached confluency simultaneously), and there were no significant differences in the cell density between the control and the active treatment arms ( $0.42 \pm 0.03 \times 10^6$  cells/cm<sup>2</sup> vs.  $0.45 \pm 0.05 \times 10^6$  cells/cm<sup>2</sup>,  $p > 0.05$ ; Supplementary Materials, Figure S1).

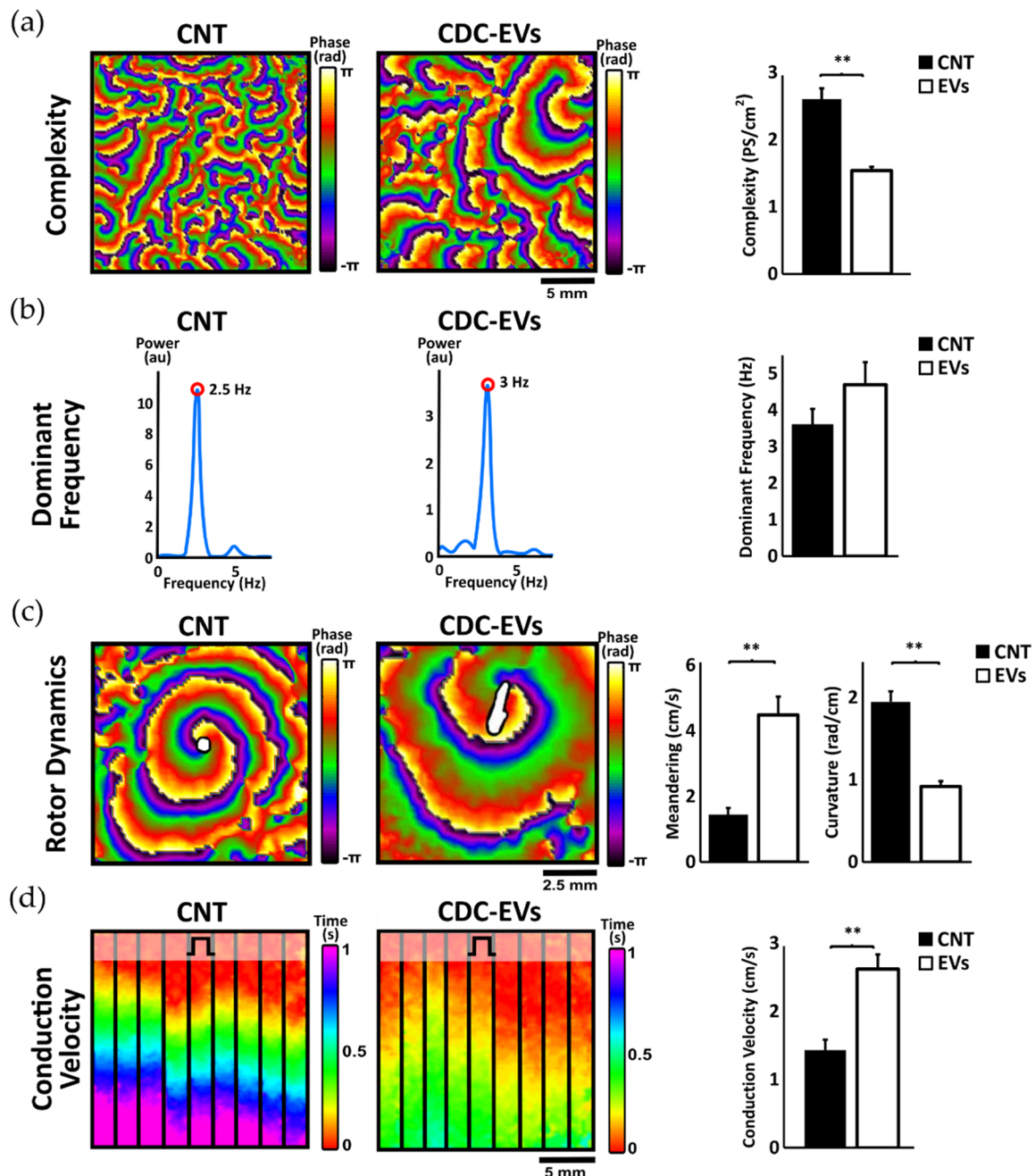


**Figure 3.** Electrophysiological characteristics comparison ( $N = 12$  in each group) and representative examples of control (CNT) and CDC-EV treated cultures. Examples of complexity, dominant frequency, rotor dynamics, and conduction velocity are illustrated for both groups. (a) Complexity was higher in the CNT vs. the CDC-EV group (\*\*  $p < 0.01$ ). (b) Average dominant frequency was not significantly different among both groups ( $p > 0.05$ ). (c) Rotor meandering was larger in the CDC-EV group vs. CNT (\*\*  $p < 0.01$ ), while curvature was smaller (\*\*  $p < 0.01$ ). (d) Conduction velocity was higher in the CDC-EV group (\*\*  $p < 0.01$ ). The isochrone map shows how the impulse took less time to travel the same distance in the CDC-EV group (500 ms) vs. the CNT group (1000 ms).

### 3.1. Effects of Extracellular Vesicles Derived from CDCs on Activation Dominant Frequency, Complexity, and Rotor Dynamics

In order to study the electrophysiological modifications of CDC-EVs on baseline arrhythmogenic substrate (spontaneously activating), dominant frequency, activation complexity, and rotor dynamics were analyzed (Figure 3). We observed a significant reduction of ~40% in the activation complexity of the CDC-EV treated group (number of phase singularity points per square centimeter,  $2.60 \pm 0.57$  vs.  $1.54 \pm 0.20$  PS/cm<sup>2</sup>,  $p < 0.01$ , Figure 3a). It can be noticed how, in the control group, there were abundant wavebreaks and secondary rotors, while, in the CDC-EV treated group, there were fewer and larger rotors, with one main rotor covering most of the dish, indicative of simpler activation patterns (Figure 3a; Supplementary Materials, Video S1). However, regarding spectral characteristics, both control and treated groups presented no significant differences in their activation rate, which was around a frequency of 4 Hz ( $3.61 \pm 1.44$  vs.  $4.69 \pm 2.15$  Hz;  $p =$  not significant; Figure 3b). CDC-EVs also induced significant differences in rotor dynamics. In particular, HL-1 monolayers treated with CDC-EVs presented significant larger spatial rotor instability in contrast to control plates, as rotors tended not to remain at fixed positions in the CDC-EV treated group. As a result, rotor meandering was significantly higher ( $1.45 \pm 0.7$  vs.  $4.48 \pm 1.95$  cm/s,  $p < 0.01$ ; Figure 3c) and presented smaller curvatures ( $1.95 \pm 0.45$  vs.  $0.92 \pm 0.23$  rad/cm,  $p < 0.01$ ; Figure 3c).

### 3.2. Extracellular Vesicles Derived from CDCs Increase Conduction Velocity in Arrhythmogenic Substrate and Increase Ion Channel Expression

Conduction velocity was assessed in HL-1 cell monocultures in linear propagations at a controlled stimulation rate of 1 Hz in the absence of spontaneous activity. Conduction velocity significantly increased by 80% in cultures treated with CDC-EVs (from  $1.43 \pm 0.53$  cm/s in the control group to  $2.62 \pm 0.75$  cm/s in the CDC-EV treated group, Figure 3d). Differences in conduction velocity can be appreciated in representative examples of linear impulse propagation in the control vs. CDC-EV group (Supplementary Materials, Video S2). As shown in the representative isochrone map in Figure 3d, the electrical impulse propagated over 1.5 cm of cell culture in ~1000 ms in the control group, while the propagation in the CDC-EVs treated group was ~500 ms.

The analysis of the relative gene expression of genes associated to relevant proteins in electrophysiological remodeling revealed a significantly higher gene expression of *SCN5A*, *CACNA1C*, and *GJA1* (coding for proteins involved in the regulation of  $I_{Na}$ ,  $I_{CaL}$ , and Cx43, respectively) in the treated group (Figure 4).

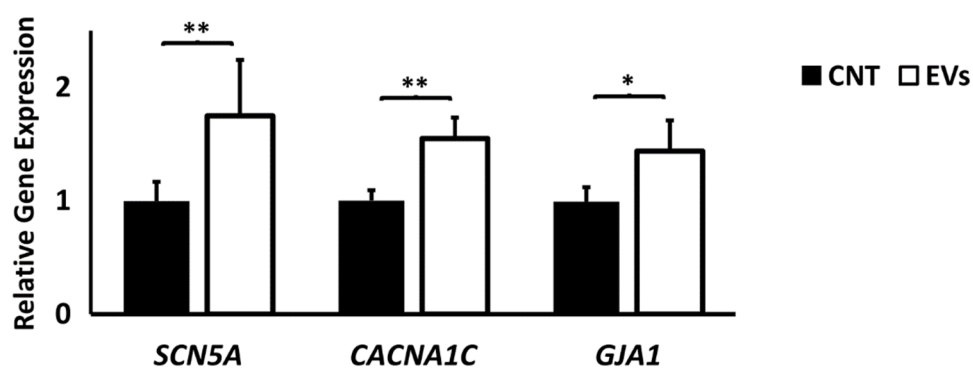


**Figure 4.** Relative gene expression results ( $N = 9$  in each group) normalized to *GUSB* and *36B4* housekeeping genes. Relative gene expression of *SCN5A* (\*\*  $p < 0.01$ ), *CACNA1C* (\*\*  $p < 0.01$ ), and *GJA1* (\*  $p < 0.05$ ) was significantly higher in the CDC-EV treated group.

To investigate the mechanism behind the reduction in complexity and the increase in conduction velocity in treated plates, gene expressions of *SCN5A*, *CACNA1C*, and *GJA1* were correlated to the electrophysiological parameters measured (Figure 5a). While *GJA1* did not show a significant



relationship, an increase in *SCN5A* and *CACNA1C* expression significantly correlated with conduction velocity ( $R^2 = 0.26$ ,  $p < 0.05$  and  $R^2 = 0.57$ ,  $p < 0.01$ , respectively), meandering ( $R^2 = 0.61$ ,  $p < 0.01$  and  $R^2 = 0.72$ ,  $p < 0.01$ ), and reduction in complexity ( $R^2 = 0.45$ ,  $p < 0.01$  and  $R^2 = 0.63$ ,  $p < 0.01$ ).

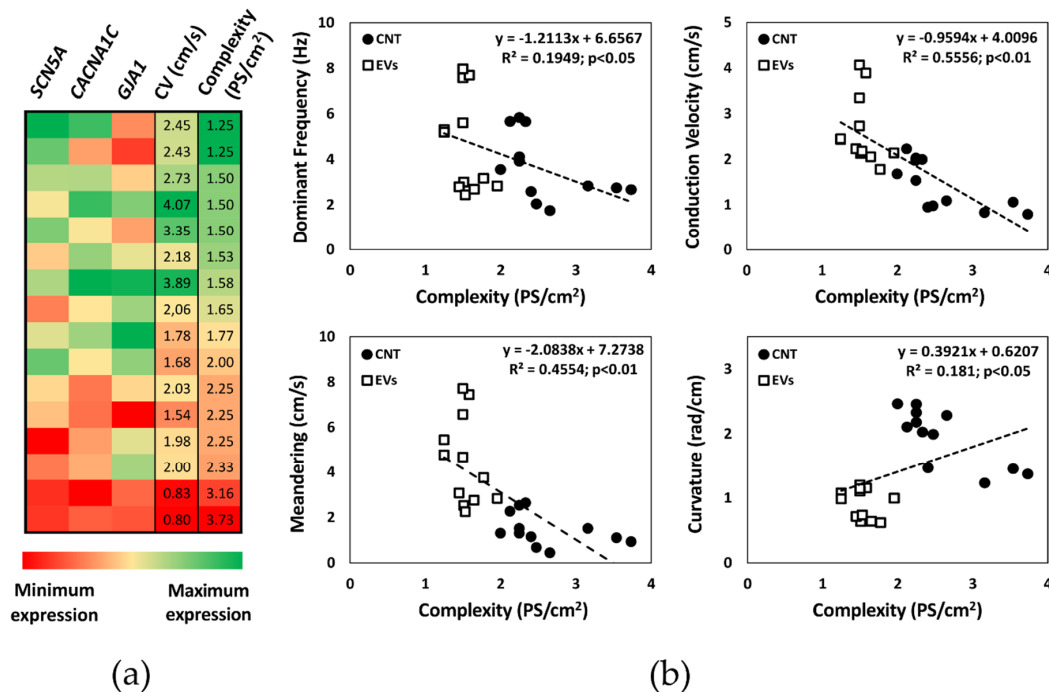


**Figure 5.** Relative gene expression relationship with CV and complexity, and relationship of the different electrophysiological parameters with activation complexity. (a) Relative gene expression of *SCN5A*, *CACNA1C*, and *GJA1* in each sample and its associated CV and complexity. While *SCN5A* and *CACNA1C* higher expression correlated significantly with higher CV and lower complexity measurements, *GJA1* expression did not. (b) Dominant frequency ( $p < 0.05$ ), CV ( $p < 0.01$ ), meandering ( $p < 0.01$ ), and curvature ( $p < 0.05$ ) correlated significantly to activation complexity.

### 3.3. Activation Complexity Electrophysiological Mechanisms

To analyze the electrophysiological mechanisms driving the reduction in the activation complexity of the arrhythmogenic substrate under CDC-EV treatment, we analyzed mean dominant frequency, rotor curvature, rotor meandering, and conduction velocity in relation to complexity (Figure 5b). Changes in complexity showed a significant correlation to dominant frequency ( $R^2 = 0.19$ ,  $p < 0.05$ ), conduction velocity ( $R^2 = 0.56$ ,  $p < 0.01$ ), meandering ( $R^2 = 0.46$ ,  $p < 0.01$ ), and curvature ( $R^2 = 0.18$ ,  $p < 0.05$ ). Higher conduction velocities, higher rotor meandering, and lower curvatures found in EV-treated plates are responsible for the reduction in the overall activation complexity. Changes in rotor movement in CDC-EV treated plates (larger meandering) are associated with a decrease in their curvature, which probably results in a larger area needed for a rotor to self-maintain. This may result in a reduction in the possible number of active rotors in a given area and, therefore, reduce the activation complexity. This higher conduction velocity and rotor meandering found in treated plates correlates with the higher expression of *SCN5A* and *CACNA1C*. This suggests that the antiarrhythmic properties of EVs are mediated by the increased expression of these genes, which modifies rotor dynamics and conduction velocity, leading to a reduction of the overall complexity of activation.

## 4. Discussion

The main finding of this study is that CDC-EVs reduce the spontaneous activation complexity of HL-1 cardiomyocytes. Our results suggest that this simplification to a less arrhythmogenic profile may

be driven by two mechanisms: the increase in the conduction velocity and the modification of rotor dynamics, correlated to a higher *SCN5A* and *CACNA1C* expression.

Low and heterogeneous conduction velocity of cardiac tissue is related to higher irregular reentry formation and probability of arrhythmic episodes [7]. Despite the fact that improving conduction velocity can reduce arrhythmogenicity under certain scenarios [9,10], no chemical drugs show strong antiarrhythmic effects through this mechanism to date [11,12]. Therefore, if confirmed in other cellular models, CDC-EVs may act as novel therapeutic conduction velocity modulators.

CDC-EVs seem to enhance the gene expression of *SCN5A*, coding for a protein directly related to  $I_{Na}$  and *GJA1*, coding for Cx43. An increase in  $I_{Na}$  conductance is related to a faster depolarization and, hence, to a higher conduction velocity of the excitable tissue [7]. The higher conduction velocity in CDC-EV treated plates may be caused by the higher expression of *SCN5A*. In contrast, Cx43, also known to play an important role in action potential propagation between cardiomyocytes and strongly linked to conduction velocity and antiarrhythmogenicity [10,13], showed a significantly higher expression in treated plates but did not correlate significantly with conduction velocity measurements. This suggests that *SCN5A* may play a dominant role in the modifications of conduction velocity in our cell model.

The second mechanism via which CDC-EVs could reduce activation complexity is by acting over rotor dynamics. Lengthening of the action potential and the refractory period is commonly associated with an increase in rotor meandering and reduction in curvature [15]. This promotes rotor instability, increasing the likelihood of collision with other rotors and enlarging the area needed for the rotor to self-maintain. As a result, the number of possible simultaneous rotors in a certain area and, therefore, the complexity decrease. A higher increase in  $I_{CaL}$  is related to larger action potential durations [16] (p. 187) and larger meandering [17]. Treated plates showed a significant higher expression of *CACNA1C* (codes for a protein related to  $I_{CaL}$ ) that correlated significantly to rotor meandering. A higher expression of *CACNA1C* could lead to a higher conductance of calcium channels and an increase in  $I_{CaL}$ , which could explain the higher rotor meandering found in CDC-EV treated plates.

Recently, Cho et al. [27] demonstrated the antiarrhythmic effects of CDCs in rats with heart failure and the preserved ejection fraction explained by the upregulation of  $I_{to}$ , homogenization of the action potential duration, and fibrosis decrease. Our results are complementary to their findings and illustrate that the antiarrhythmic effect of CDC-EVs is mediated both by an increase in conduction velocity and by modification of rotor dynamics. Our results open new perspectives into the unraveling of the antiarrhythmic properties of CDCs.

This study used HL-1 cardiomyocyte monolayers as models of arrhythmic substrate. Despite being an in vitro cell line capable of presenting a mature cardiac phenotype and being widely used to study cardiac electrophysiology and arrhythmias [39,40,42–49], their use has several limitations that must be taken into account. HL-1 cells, although being mature, are of murine origin and present important electrophysiological differences with adult human cardiac tissue. In fact, the expression of genes related to potassium currents (such as  $I_{K1}$ ) could not be analyzed in our study due to the extremely low expression. Monolayers also represent an in vitro two-dimensional (2D) scenario that aims to represent a more complex three-dimensional (3D) in vivo environment. In addition to that, since HL-1 cultures present spontaneous arrhythmogenic activity, it is not possible to observe the complete elimination of spontaneous activations under the effect of EVs. Although gene expression patterns were used to investigate potential mechanisms of actions, we should not consider gene expression as a surrogate of protein expression, since they do not necessarily correlate under all circumstances.

Considering these limitations, future studies should be directed toward validation of the increase in conduction velocity, rotor meandering, and reduction in complexity of CDC-EVs in other cell models and human samples. Protein expression should also be investigated to support the possible mechanism of action behind the influence of CDC-EVs on the electrophysiological properties of cardiomyocytes.

## 5. Conclusions

CDC-EVs reduce the spontaneous activation complexity of HL-1 cardiomyocytes, leading to a less arrhythmogenic profile. If validated in other cellular models, CDC-EVs may be used specifically as antiarrhythmic agents in a wide range of cardiac pathologies.

**Supplementary Materials:** The following are available online at <http://www.mdpi.com/2227-9717/8/8/924/s1>: Table S1. Primers used for RT-PCR; Figure S1. Representative images of the HL-1 culture at 100% confluency on day 4 of the experiment in control and CDC-EVs groups; Video S1. Activation complexity recording in a representative example of a control culture vs. a CDC-EV treated culture; Video S2. Conduction velocity recording in a representative example of a control culture vs. a CDC-EV treated culture.

**Author Contributions:** Conceptualization, L.G.-C., I.H.-R. and L.G.-S.; methodology, L.G.-C., M.M.-L., A.S.d.l.N., A.I.F. and S.S.-S.; software, L.G.-C., M.M.-L., A.S.d.l.N. and I.H.-R.; validation, L.G.-S.; formal analysis, L.G.-C. and M.M.-L.; investigation, L.G.-C. and M.M.-L.; data curation, L.G.-C. and M.M.-L.; writing—original draft preparation, L.G.-C.; writing—review and editing, M.M.-L., A.S.d.l.N., I.H.-R., A.I.F., F.A., L.G.-S. and F.F.-A.; visualization, L.G.-C., M.M.-L. and L.G.-S.; supervision, L.G.-S.; project administration, L.G.-S. and F.F.-A.; funding acquisition, F.F.-A. All authors read and agreed to the published version of the manuscript.

**Funding:** This research was funded by the Instituto de Salud Carlos III, Ministerio de Ciencia e Innovación, Spain: PI16/01123, PI17/01059, Red de Terapia Celular—Tercel—RD16.0011.0029 and CIBERCV—CB16.11.00292.

**Conflicts of Interest:** The authors declare no conflicts of interest. The funders had no role in the design of the study; in the collection, analyses, or interpretation of data; in the writing of the manuscript, or in the decision to publish the results.

## References

1. Antzelevitch, C.; Burashnikov, A. Overview of Basic Mechanisms of Cardiac Arrhythmia. *Card. Electrophysiol. Clin.* **2011**, *3*, 23–45. [[CrossRef](#)] [[PubMed](#)]
2. Perna, F.; Leo, M. Epidemiology, Classification and Description of Cardiac Arrhythmias. In *Sports Cardiology: From Diagnosis to Clinical Management*; Fioranelli, M., Frajese, G., Eds.; Springer: Milan, Italy, 2012; pp. 155–177.
3. Khurshid, S.; Choi, S.H.; Weng, L.-C.; Wang, E.Y.; Trinquart, L.; Benjamin, E.J.; Ellinor, P.T.; Lubitz, S.A. Frequency of Cardiac Rhythm Abnormalities in a Half Million Adults. *Circ. Arrhythm. Electrophysiol.* **2018**, *11*, e006273. [[CrossRef](#)] [[PubMed](#)]
4. Macle, L.; Nattel, S. Arrhythmias in 2015: Advances in drug, ablation, and device therapy for cardiac arrhythmias. *Nat. Rev. Cardiol.* **2016**, *13*, 67–68. [[CrossRef](#)] [[PubMed](#)]
5. Gopinathannair, R.; Olshansky, B. Management of tachycardia. *F1000Prime Rep.* **2015**, *7*. [[CrossRef](#)]
6. Cho, H.C.; Marbán, E. Biological therapies for cardiac arrhythmias: Can genes and cells replace drugs and devices? *Circ. Res.* **2010**, *106*, 674–685. [[CrossRef](#)]
7. King, J.H.; Huang, C.L.-H.; Fraser, J.A. Determinants of myocardial conduction velocity: Implications for arrhythmogenesis. *Front. Physiol.* **2013**, *4*. [[CrossRef](#)]
8. Aronis Konstantinos, N.; Berger Ronald, D. Ashikaga Hiroshi Rotors. *Circ. Arrhythm. Electrophysiol.* **2017**, *10*, e005634.
9. Lau, D.H.; Clausen, C.; Sosunov, E.A.; Shlapakova, I.N.; Anyukhovskiy, E.P.; Danilo, P.; Rosen, T.S.; Kelly, C.; Duffy, H.S.; Szabolcs, M.J.; et al. Epicardial border zone overexpression of skeletal muscle sodium channel SkM1 normalizes activation, preserves conduction, and suppresses ventricular arrhythmia: An in silico, in vivo, in vitro study. *Circulation* **2009**, *119*, 19–27. [[CrossRef](#)]
10. Igarashi, T.; Finet, J.E.; Takeuchi, A.; Fujino, Y.; Strom, M.; Greener, I.D.; Rosenbaum, D.S.; Donahue, J.K. Connexin gene transfer preserves conduction velocity and prevents atrial fibrillation. *Circulation* **2012**, *125*, 216–225. [[CrossRef](#)]
11. Golan, D.E.; Tashjian, A.H.; Armstrong, E.J. *Principles of Pharmacology: The Pathophysiologic Basis of Drug Therapy*; Lippincott Williams & Wilkins: Philadelphia, PA, USA, 2011.
12. Haugan, K.; Miyamoto, T.; Takeishi, Y.; Kubota, I.; Nakayama, J.; Shimojo, H.; Hirose, M. Rotigaptide (ZP123) Improves Atrial Conduction Slowing in Chronic Volume Overload-Induced Dilated Atria. *Basic Clin. Pharmacol. Toxicol.* **2006**, *99*, 71–79. [[CrossRef](#)]
13. Roell, W.; Lewalter, T.; Sasse, P.; Tallini, Y.N.; Choi, B.-R.; Breitbach, M.; Doran, R.; Becher, U.M.; Hwang, S.-M.; Bostani, T.; et al. Engraftment of connexin 43-expressing cells prevents post-infarct arrhythmia. *Nature* **2007**, *450*, 819–824. [[CrossRef](#)] [[PubMed](#)]

14. Rossello, R.A.; Kohn, D.H. Gap Junction Intercellular Communication: A Review of a Potential Platform to Modulate Craniofacial Tissue Engineering. *J. Biomed. Mater. Res. B Appl. Biomater.* **2009**, *88*, 509–518. [[CrossRef](#)] [[PubMed](#)]
15. Comtois, P.; Kneller, J.; Nattel, S. Of circles and spirals: Bridging the gap between the leading circle and spiral wave concepts of cardiac reentry. *Europace* **2005**, *7* (Suppl. 2), 10–20. [[CrossRef](#)] [[PubMed](#)]
16. Cha, Y.-M.; Friedman, P.A. *Mayo Clinic Electrophysiology Manual*; Oxford University Press: Oxford, UK, 2013.
17. Qu, Z.; Xie, F.; Garfinkel, A.; Weiss, J. Origins of Spiral Wave Meander and Breakup in a Two-Dimensional Cardiac Tissue Model. *Ann. Biomed. Eng.* **2000**, *28*, 755–771. [[CrossRef](#)]
18. Zipes, D.P.; Jalife, J. *Cardiac Electrophysiology: From Cell to Bedside E-Book: Expert Consult*; Elsevier Health Sciences: Amsterdam, The Netherlands, 2009.
19. Lim, H.S.; Hocini, M.; Dubois, R.; Denis, A.; Derval, N.; Zellerhoff, S.; Yamashita, S.; Berte, B.; Mahida, S.; Komatsu, Y.; et al. Complexity and Distribution of Drivers in Relation to Duration of Persistent Atrial Fibrillation. *J. Am. Coll. Cardiol.* **2017**, *69*, 1257–1269. [[CrossRef](#)]
20. Albert, C.M.; Stevenson, W.G. The Future of Arrhythmias and Electrophysiology. *Circulation* **2016**, *133*, 2687–2696. [[CrossRef](#)]
21. Raymond-Paquin, A.; Andrade, J.; Macle, L. Catheter ablation: An ongoing revolution. *J. Thorac. Dis.* **2019**, *11*, S212–S215. [[CrossRef](#)]
22. Sadraddin, H.; Gaebel, R.; Skorska, A.; Lux, C.A.; Sasse, S.; Ahmad, B.; Vasudevan, P.; Steinhoff, G.; David, R. CD271+ Human Mesenchymal Stem Cells Show Antiarrhythmic Effects in a Novel Murine Infarction Model. *Cells* **2019**, *8*, 1474. [[CrossRef](#)]
23. Park, H.; Park, H.; Mun, D.; Kang, J.; Kim, H.; Kim, M.; Cui, S.; Lee, S.-H.; Joung, B. Extracellular Vesicles Derived from Hypoxic Human Mesenchymal Stem Cells Attenuate GSK3 $\beta$  Expression via miRNA-26a in an Ischemia-Reperfusion Injury Model. *Yonsei Med. J.* **2018**, *59*, 736–745. [[CrossRef](#)]
24. Mayourian, J.; Cashman, T.J.; Ceholski, D.K.; Johnson, B.V.; Sachs, D.; Kaji, D.A.; Sahoo, S.; Hare, J.M.; Hajjar, R.J.; Sobie, E.A.; et al. Experimental and Computational Insight Into Human Mesenchymal Stem Cell Paracrine Signaling and Heterocellular Coupling Effects on Cardiac Contractility and Arrhythmogenicity. *Circ. Res.* **2017**, *121*, 411–423. [[CrossRef](#)]
25. Hwang, H.J.; Chang, W.; Song, B.-W.; Song, H.; Cha, M.-J.; Kim, I.-K.; Lim, S.; Choi, E.J.; Ham, O.; Lee, S.-Y.; et al. Antiarrhythmic potential of mesenchymal stem cell is modulated by hypoxic environment. *J. Am. Coll. Cardiol.* **2012**, *60*, 1698–1706. [[CrossRef](#)] [[PubMed](#)]
26. Ramireddy, A.; Brodt, C.R.; Mendizabal, A.M.; DiFede, D.L.; Healy, C.; Goyal, V.; Alansari, Y.; Coffey, J.O.; Viles-Gonzalez, J.F.; Heldman, A.W.; et al. Effects of Transendocardial Stem Cell Injection on Ventricular Proarrhythmia in Patients with Ischemic Cardiomyopathy: Results from the POSEIDON and TAC-HFT Trials. *Stem Cells Transl. Med.* **2017**, *6*, 1366–1372. [[CrossRef](#)] [[PubMed](#)]
27. Cho, J.H.; Kilfoil, P.J.; Zhang, R.; Solymani, R.E.; Bresee, C.; Kang, E.M.; Luther, K.; Rogers, R.G.; de Couto, G.; Goldhaber, J.I.; et al. Reverse electrical remodeling in rats with heart failure and preserved ejection fraction. *JCI Insight* **2018**, *3*. [[CrossRef](#)]
28. Cho, J.H.; Kilfoil, P.J.; Solymani, R.; Luther, K.; Rogers, R.G.; de Couto, G.; Zhang, R.; Sanchez, L.; Goldhaber, J.I.; Marban, E.; et al. Abstract 15421: Anti-Arrhythmic Effects of Heart-Derived Cell Therapy in a Rat Model of Heart Failure With Preserved Ejection Fraction. *Circulation* **2017**, *136*, A15421. [[CrossRef](#)] [[PubMed](#)]
29. Askar, S.F.A.; Ramkisoensing, A.A.; Atsma, D.E.; Schalij, M.J.; de Vries, A.A.F.; Pijnappels, D.A. Engraftment patterns of human adult mesenchymal stem cells expose electrotonic and paracrine proarrhythmic mechanisms in myocardial cell cultures. *Circ. Arrhythm. Electrophysiol.* **2013**, *6*, 380–391. [[CrossRef](#)]
30. Eun, L.Y.; Song, H.; Choi, E.; Lee, T.G.; Moon, D.W.; Hwang, D.; Byun, K.H.; Sul, J.H.; Hwang, K.C. Implanted bone marrow-derived mesenchymal stem cells fail to metabolically stabilize or recover electromechanical function in infarcted hearts. *Tissue Cell* **2011**, *43*, 238–245. [[CrossRef](#)]
31. Raposo, G.; Stoorvogel, W. Extracellular vesicles: Exosomes, microvesicles, and friends. *J. Cell Biol.* **2013**, *200*, 373–383. [[CrossRef](#)]
32. Marbán, E. The Secret Life of Exosomes: What Bees Can Teach Us About Next-Generation Therapeutics. *J. Am. Coll. Cardiol.* **2018**, *71*, 193–200. [[CrossRef](#)]
33. Ibrahim, A.G.-E.; Cheng, K.; Marbán, E. Exosomes as Critical Agents of Cardiac Regeneration Triggered by Cell Therapy. *Stem Cell Rep.* **2014**, *2*, 606–619. [[CrossRef](#)]

34. Chen, B.; Li, Q.; Zhao, B.; Wang, Y. Stem Cell-Derived Extracellular Vesicles as a Novel Potential Therapeutic Tool for Tissue Repair. *Stem Cells Transl. Med.* **2017**, *6*, 1753–1758. [[CrossRef](#)]
35. Makkar, R.R.; Smith, R.R.; Cheng, K.; Malliaras, K.; Thomson, L.E.; Berman, D.; Czer, L.S.; Marbán, L.; Mendizabal, A.; Johnston, P.V.; et al. Intracoronary cardiosphere-derived cells for heart regeneration after myocardial infarction (CADUCEUS): A prospective, randomised phase 1 trial. *Lancet* **2012**, *379*, 895–904. [[CrossRef](#)]
36. Grigorian-Shamagian, L.; Liu, W.; Fereydooni, S.; Middleton, R.C.; Valle, J.; Cho, J.H.; Marbán, E. Cardiac and systemic rejuvenation after cardiosphere-derived cell therapy in senescent rats. *Eur. Heart J.* **2017**, *38*, 2957–2967. [[CrossRef](#)] [[PubMed](#)]
37. Smith, R.R.; Barile, L.; Cho, H.C.; Leppo, M.K.; Hare, J.M.; Messina, E.; Giacomello, A.; Abraham, M.R.; Marbán, E. Regenerative potential of cardiosphere-derived cells expanded from percutaneous endomyocardial biopsy specimens. *Circulation* **2007**, *115*, 896–908. [[CrossRef](#)] [[PubMed](#)]
38. Claycomb, W.C.; Lanson, N.A.; Stallworth, B.S.; Egeland, D.B.; Delcarpio, J.B.; Bahinski, A.; Izzo, N.J. HL-1 cells: A cardiac muscle cell line that contracts and retains phenotypic characteristics of the adult cardiomyocyte. *Proc. Natl. Acad. Sci. USA* **1998**, *95*, 2979–2984. [[CrossRef](#)] [[PubMed](#)]
39. Climent, A.M.; Guillem, M.S.; Fuentes, L.; Lee, P.; Bollensdorff, C.; Fernández-Santos, M.E.; Suárez-Sancho, S.; Sanz-Ruiz, R.; Sánchez, P.L.; Aienza, F.; et al. Role of atrial tissue remodeling on rotor dynamics: An in vitro study. *Am. J. Physiol. Heart Circ. Physiol.* **2015**, *309*, H1964–H1973. [[CrossRef](#)]
40. Del-Canto, I.; Gómez-Cid, L.; Hernández Romero, I.; Guillem, M.S.; Fernández-Santos, E.; Aienza, F.; Such, L.; Fernández-Avilés, F.; Chorro, F.J.; Climent, A.M. Ranolazine-mediated Attenuation of Mechanoelectric Feedback in Atrial Myocyte Monolayers. *Front. Physiol.* **2020**, *11*, 922.
41. Vandesompele, J.; De Preter, K.; Pattyn, F.; Poppe, B.; Van Roy, N.; De Paepe, A.; Speleman, F. Accurate normalization of real-time quantitative RT-PCR data by geometric averaging of multiple internal control genes. *Genome Biol.* **2002**, *3*, research0034.1. [[CrossRef](#)]
42. Van Gorp, P.R.R.; Trines, S.A.; Pijnappels, D.A.; de Vries, A.A.F. Multicellular In vitro Models of Cardiac Arrhythmias: Focus on Atrial Fibrillation. *Front. Cardiovasc. Med.* **2020**, *7*. [[CrossRef](#)]
43. Brundel, B.J.J.M.; Kampinga, H.H.; Henning, R.H. Calpain inhibition prevents pacing-induced cellular remodeling in a HL-1 myocyte model for atrial fibrillation. *Cardiovasc. Res.* **2004**, *62*, 521–528. [[CrossRef](#)]
44. Hong, J.; Choi, J.H.; Kim, T.Y.; Lee, K.-J. Spiral reentry waves in confluent layer of HL-1 cardiomyocyte cell lines. *Biochem. Biophys. Res. Commun.* **2008**, *377*, 1269–1273. [[CrossRef](#)]
45. Mace, L.C.; Yermalitskaya, L.V.; Yi, Y.; Yang, Z.; Murray, K.T. Transcriptional Remodeling of Rapidly Stimulated HL-1 Atrial Myocytes Exhibits Concordance with Human Atrial Fibrillation. *J. Mol. Cell Cardiol.* **2009**, *47*, 485–492. [[CrossRef](#)] [[PubMed](#)]
46. Tsai, C.-T.; Chiang, F.-T.; Chen, W.-P.; Hwang, J.-J.; Tseng, C.-D.; Wu, C.-K.; Yu, C.-C.; Wang, Y.-C.; Lai, L.-P.; Lin, J.-L. Angiotensin II induces complex fractionated electrogram in a cultured atrial myocyte monolayer mediated by calcium and sodium-calcium exchanger. *Cell Calcium* **2011**, *49*, 1–11. [[CrossRef](#)] [[PubMed](#)]
47. Tsai, C.-T.; Chiang, F.-T.; Tseng, C.-D.; Yu, C.-C.; Wang, Y.-C.; Lai, L.-P.; Hwang, J.-J.; Lin, J.-L. Mechanical stretch of atrial myocyte monolayer decreases sarcoplasmic reticulum calcium adenosine triphosphatase expression and increases susceptibility to repolarization alternans. *J. Am. Coll. Cardiol.* **2011**, *58*, 2106–2115. [[CrossRef](#)] [[PubMed](#)]
48. Dias, P.; Desplantez, T.; El-Harasis, M.A.; Chowdhury, R.A.; Ullrich, N.D.; Cabestrero de Diego, A.; Peters, N.S.; Severs, N.J.; MacLeod, K.T.; Dupont, E. Characterisation of connexin expression and electrophysiological properties in stable clones of the HL-1 myocyte cell line. *PLoS ONE* **2014**, *9*, e90266. [[CrossRef](#)]
49. Houston, C.; Tzortzis, K.N.; Roney, C.; Saglietto, A.; Pitcher, D.S.; Cantwell, C.D.; Chowdhury, R.A.; Ng, F.S.; Peters, N.S.; Dupont, E. Characterisation of re-entrant circuit (or rotational activity) in vitro using the HL1-6 myocyte cell line. *J. Mol. Cell. Cardiol.* **2018**, *119*, 155–164. [[CrossRef](#)]

